Taylor & Francis
Taylor & Francis Group

Decoupling features for fault detection and diagnosis on centrifugal chillers (1486-RP)

Xinzhi Zhao,* Mo Yang, and Haorong Li
University of Nebraska-Lincoln, Architectural Engineering, Omaha, NE, USA
**Corresponding author e-mail: xinzhizhao@unomaha.edu*

With growing realization of the benefits brought by fault detection and diagnosis(FDD), a large body of research pertinent to FDD methods for centrifugal chillers has been conducted during the past two decades. However, at the present time, relatively few FDD methods can handle multiple simultaneous faults on centrifugal chillers. This article describes the development of some decoupling features, which are the basis of a decoupling-based FDD methodology that can handle multiple simultaneous faults on centrifugal chillers. The performance of the decoupling features were validated and evaluated by the laboratory data from a 90-ton centrifugal chiller tested in a laboratory environment.

Introduction

Buildings consume more and more energy— currently about 73% of electricity and 40% of primary energy in the United States (DOE 2009). Among various building energy systems, centrifugal chillers are large contributors of energy usage and maintenance costs for HVAC systems. The performance of centrifugal chiller degrades gradually due to faults introduced during initial installation or developed in routine operation. The parasitical faults in chiller systems lead to inefficient operation, degraded performance, additional maintenance costs, and shorter equipment longevity. Fault detection and diagnosis (FDD) technology has the potential to guard against faults, reducing energy penalty, equipment downtime, and maintenance costs.

During the past 20 years, a large body of systematic FDD research on chiller systems has been conducted. To meet imperative needs for a comprehensive study of automated FDD for centrifugal chillers, a three-phase research project for development, evaluation, and laboratory and field testing of FDD methods for centrifugal chillers has been sponsored by ASHRAE since 1998. The first phase (1043-RP; Comstock and Braun 1999) identified some common and important faults for centrifugal chillers based upon frequency of service and maintenance costs; a database of chiller performance was built for fault-free and faulty operation under different levels of fault severity and different operating conditions on a 90-ton laboratory centrifugal chiller. The second phase (1275-RP, Reddy 2006) was initiated to evaluate the effectiveness and robustness of four promising FDD methods using the tools provided by 1043-RP (Comstock and Braun 1999) and to identify which was the most promising for subsequent field evaluation and adoption, as well as to develop a general and practical evaluation methodology for assessing the performance of FDD methods. Jia and Reddy (2003) proposed a generic model-based FDD method for chillers using characteristic features that are sensitive to some faults. Similar to the multivariate regression method

Received April 18, 2010; accepted September 27, 2010
Xinzhi Zhao is a PhD Student. **Mo Yang** is a PhD Student. **Haorong Li, PhD**, is Associate Professor.

HVAC&R Research, 17(1):86–106, 2011.
ISSN: 1078-9669 print / 1938-5587 online
DOI: 10.1080/10789669.2011.543254

evaluated by Reddy (2007a), a simple regression model-based FDD method for large chillers was presented by Reddy (2007b). The simple regression model using only a thermal load as a regressor to describe the changes of characteristic features under different operating conditions was developed. The model predictions were compared with actual performance data to generate the residuals, which were used to detect and diagnose faults. Wang and Cui (2006) proposed a strategy that which consisted of a model-based chiller FDD scheme to handle typical chiller faults. The chiller FDD scheme was developed based on six performance indices, which were deduced from theoretical analysis to characterize the health condition of centrifugal chillers.

Many existing FDD methods have good performance in handling faults that happen individually. However, the existing FDD methods for centrifugal chillers can hardly deal with multiple faults that happen concurrently. Li and Braun (2007a) developed a decoupling-based (DB) FDD (DB-FDD) method for vapor compression cycle equipment to handle the multiple-simultaneous faults. The DB-FDD method has been implemented on a package unit system in both laboratory and field environments, which demonstrated its accurate and robust performance. The key to handling multiple simultaneous faults lies in identifying the decoupling features, which are uniquely dependent on individual faults (Li and Braun 2007b). The decoupling features can also be used as virtual sensors to monitor and diagnose faults in vapor compression air conditioners (Li and Braun 2009a, 2009b, 2009c). The centrifugal chiller also uses the vapor compression cycle and experiences certain faults encountered by package vapor compression units, such as low refrigerant charge, refrigerant overcharge, noncondensable gas in refrigerant, etc. However, there are some differences between package unit system and centrifugal chillers system, for example, the different refrigerant mass flow rate control method, different heat exchanger type, different refrigerant cool method, different symptom of faults, etc. Therefore, the decoupling features for package unit system can hardly be applied directly to centrifugal chillers. The key point of applying the DB-FDD method in centrifugal chillers is to identify the decoupling features specifically pertinent to centrifugal chiller systems.

This article developed some decoupling features for common faults that occur in centrifugal chillers, and the detailed strategy for developing those decoupling features is presented. Finally, the performance of the developed decoupling features were validated and evaluated with the laboratory data from a 90-ton chiller tested in a laboratory environment.

Methodology of DB-FDD method

To handle the multiple-simultaneous faults, Li and Braun (2007a) formulated model-based FDD techniques in a general mathematical way (Equation 1) and found that decoupling is the key to handle multiple-simultaneous faults. As shown in Equation 2, the decoupling methodology transforms a complicated multiple-input and multiple-output FDD problem into a finite number of simple single-input and single-output problems. That is, a fault indicator termed the decoupling feature is uniquely related to a single fault and is independent of the impacts of other faults and driving conditions. Consequently, multiple faults can be handled;

$$\begin{bmatrix} variable\ 1 \\ variable\ 2 \\ \vdots \\ variable\ i \\ \vdots \\ variable\ n \end{bmatrix} = \begin{bmatrix} f_{11}(\cdot) & f_{12}(\cdot) & \cdots & f_{1i}(\cdot) & \cdots & f_{1n}(\cdot) \\ f_{21}(\cdot) & f_{22}(\cdot) & \cdots & f_{2i}(\cdot) & \cdots & f_{2n}(\cdot) \\ \vdots & \vdots & \ddots & \vdots & \ddots & \vdots \\ f_{i1}(\cdot) & f_{i2}(\cdot) & \cdots & f_{ii}(\cdot) & \cdots & f_{in}(\cdot) \\ \vdots & \vdots & \ddots & \vdots & \ddots & \vdots \\ f_{n1}(\cdot) & f_{n2}(\cdot) & \cdots & f_{ni}(\cdot) & \cdots & f_{nn}(\cdot) \end{bmatrix} \times \begin{bmatrix} fault\ 1 \\ fault\ 2 \\ \vdots \\ fault\ i \\ \vdots \\ fault\ n \end{bmatrix}, \quad (1)$$

where *variable i* represents a certain state variable of the diagnosed system (e.g., subcooling), *fault i* represents a certain fault of the diagnosed system (e.g., refrigerant overcharge), and $f_{ij}(\cdot)$ denotes the

function relationship between *fault j* and *variable i*;

$$\begin{bmatrix} feature\ 1 \\ feature\ 2 \\ \vdots \\ feature\ i \\ \vdots \\ feature\ n \end{bmatrix} = \begin{bmatrix} f_{11}(\cdot) & & & & \\ & f_{22}(\cdot) & & & \\ & & \ddots & & \\ & & & f_{ii}(\cdot) & \\ & & & & \ddots \\ & & & & f_{nn}(\cdot) \end{bmatrix} \times \begin{bmatrix} fault\ 1 \\ fault\ 2 \\ \vdots \\ fault\ i \\ \vdots \\ fault\ n \end{bmatrix}, \quad (2)$$

where *feature i* represents a decoupling feature for *fault i*, and $f_{ii}(\cdot)$ denotes the function relationship between *fault i* and *feature i*.

It is obvious that full decoupling can easily handle multiple simultaneous faults, but the criterion of full decoupling is not a necessary condition and can be lowered. The worst case can be handled as shown in Equation 3, in which *feature i* can only be affected by *fault j*, where $j \leq I$; partial decoupling is sufficient for an FDD application;

$$\begin{bmatrix} feature\ 1 \\ feature\ 2 \\ \vdots \\ feature\ n \end{bmatrix} = \begin{bmatrix} f_{11}(\cdot) & & & \\ f_{21}(\cdot) & f_{22}(\cdot) & & \\ \vdots & \vdots & \ddots & \\ f_{n1}(\cdot) & f_{n2}(\cdot) & \cdots & f_{nn}(\cdot) \end{bmatrix} \begin{bmatrix} fault\ 1 \\ fault\ 2 \\ \vdots \\ fault\ n \end{bmatrix}. \quad (3)$$

From the above mathematical derivation, it can be seen that the key to handling the multiple simultaneous faults lies in identifying the decoupling features, which are uniquely dependent on individual faults. Theoretically, an infinite number of decoupled-feature sets can be constructed mathematically as long as detailed system models are available. But, in fact, limited by physical conditions, the detailed system models are hard and cost prohibitive to build, so the desired decoupling features are difficult to develop. To address this problem, Li and Braun (2007a) developed a non-mathematical decoupling approach that is based on individual component modeling and various conceptual decoupling to identify decoupling features. The taxonomy methodology was involved in the approach to address and decouple the interactions among different faults. From microscopic and macroscopic points of view, Li and Braun (2007a) categorized seven common rooftop units' faults into two classes: component-level faults and system-level faults. The characteristic of component-level faults is that their source impact can be confined to a component. The source impact here means the direct impact from the fault. On the contrary, the source impact of system-level faults cannot be confined to a specific component. So, decoupling of component-level and system-level faults can be achieved by investigating their source impacts, respectively. From a fault cause point of view, the common rooftop units' faults are divided into operational faults and service faults. Operational faults usually develop during normal running and occur randomly or gradually, while service faults are introduced with service. Since the service faults can be detected, diagnosed, and repaired immediately after installation or service, they will not occur simultaneously with operational faults. Therefore, coupling between service faults and operational faults can be decoupled.

Under the guide of the decoupling methodology, decoupling features for six common chiller faults were developed in this study.

Taxonomy of common faults in centrifugal chillers

To find decoupling features, it is necessary to have a comprehensive understanding on the common chiller faults. A taxonomy of common chiller faults would contribute to grasping the interactions among different faults, which provides a guide to find the desired decoupling features.

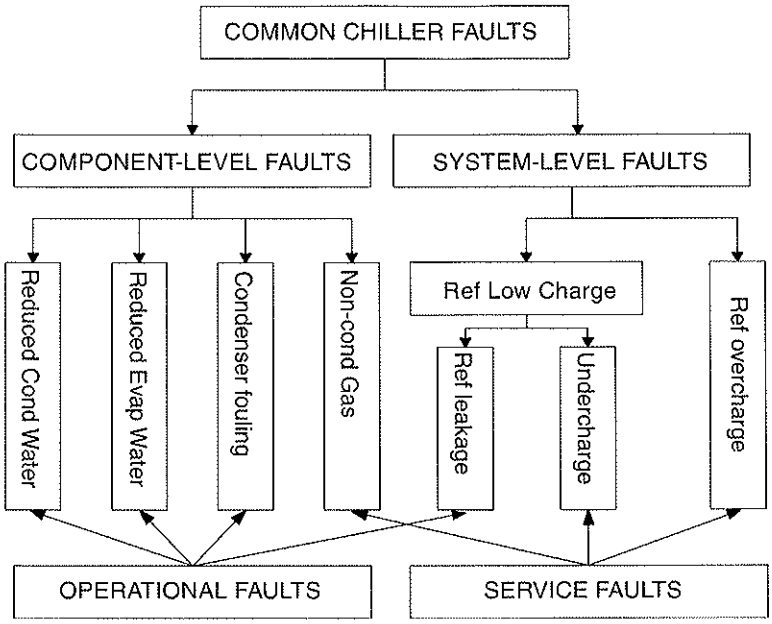

Figure 1. Taxonomy of chiller faults.

As shown in Figure 1, six common chiller faults (reduced condenser water flow rate, reduced evaporator water flow rate, low refrigerant charge, refrigerant overcharge, condenser fouling, noncondensable gas) were divided into two categories: component-level faults and system-level faults. From the fault cause point of view, they were divided into operational faults and service faults.

The reduced condenser water flow rate fault, just as its name implies, is a component-level fault. Reducing the condenser water flow rate at a constant condenser entering water temperature would raise the condenser water leaving temperature, hence causing higher condenser temperature and pressure, thereby leading the compressor to work harder and draw more power. Since the reduced condenser water flow rate fault happens and develops when the system is running, it is classified as an operational fault.

Similar to the reduced condenser water flow rate fault, the reduced evaporator water flow rate is also a component-level and operational fault.

Since most centrifugal chillers run under a positive pressure condition after being charged (typically, R134A is used in centrifugal chillers), the noncondensable-gases fault is usually introduced during the service period. Moreover, the noncondensable gas tends to accumulate in the condenser. Its primary effect is to increase heat transfer resistance, resulting in high condenser pressure and temperature. Therefore, the noncondensable gas is considered to be a component-level service fault.

In water-cooled centrifugal chillers, fouling accumulates gradually in the condenser tubes regardless of the water treatment processes employed. Hard deposits, such as scale, significantly affects the heat transfer within the condenser, which leads to increased energy consumption of the compressor. Physically, this impact is confined to the condenser component. In addition, the condenser fouling fault develops slowly when the system is running, so it is classified as a component-level and operational fault.

The low refrigerant charge and the refrigerant overcharge is a system-level fault, since these two faults can occur anywhere in the system and the direct impact cannot be confined to certain particular location. For refrigerant overcharge fault, it usually happens during service, so it is a service fault. Refrigerant low charge has two possible causes: refrigerant is undercharged or refrigerant leakage happens. Therefore, low charge can be either a system-level operational fault or a service fault.

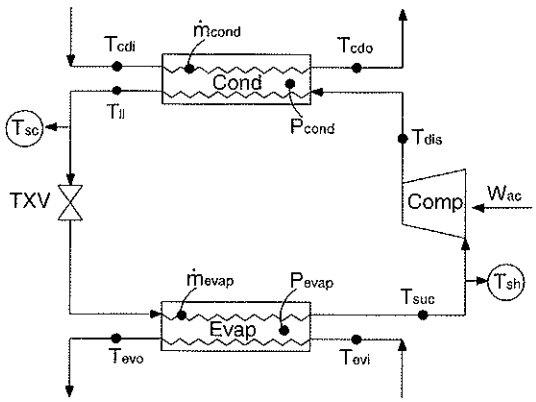

Figure 2. Required sensor information for decoupling features.

Development of decoupling features for centrifugal chiller system

Based on DB methodology, the decoupling features for six common chiller faults were developed in this study: (1) reduced condenser water flow, (2) reduced evaporator water flow, (3) low refrigerant charge, (4) refrigerant overcharge, (5) noncondensable gas in the refrigerant, and (6) condenser fouling. The actual measurements (bare symbols) and derived variables (circled symbols) used in the methodology are shown in Figure 2. The required measurements are common onboard measurements in the field.

Figure 3 describes the sequence of steps used to implement the proposed methodology. Decoupling features for the reduced condenser water flow fault and the reduced evaporator water flow fault will run first. At this step, the condenser and evaporator water flow in the chiller can be monitored, and the estimated condenser water flow rate will be used for the other decoupling features. Once a reduced condenser water flow fault is detected, the fault will be verified and removed. If the condenser water flow is normal, the decoupling feature for noncondensable gas will run. Once a noncondensable gas fault is found, the fault will be repaired immediately. If the feature does not detect a noncondensable gas fault, the decoupling features for condenser fouling, low refrigerant charge, and refrigerant overcharge faults will run to detect and diagnose corresponding chiller faults. The strategies of decoupling features are described in the following.

Component-level faults decoupling

Decoupling feature for reduced condenser water flow rate fault

Usually the condenser water flow rate is kept at constant; the comparison between actual condenser water flow rate and rated condenser water flow rate could be chosen as an independent feature for reduced condenser water flow rate fault.

For water flow rate reduction fault, the most straightforward method is to insert a water flow meter in the water loop to monitor water flow rate directly. However, expensive initial costs and requirements of continuous maintenance and calibration limit the application of the water flow meter in the field. In this study, a virtual water flow meter was developed to monitor the water flow rate in the system.

Applying energy balance theory on the condenser, the condenser water flow rate can be expressed as follows:

$$\dot{m}_{cond} = \frac{\dot{m}_r \times (h_{dis} - h_{ll})}{c_p \times (T_{cdo} - T_{cdi})}, \tag{4}$$

where $\dot{m}_r$ is the refrigerant mass flow rate, h_{dis} is the refrigerant enthalpy at the compressor outlet, h_{ll} is the condenser outlet enthalpy, $\dot{m}_{cond}$ is the condenser water flow rate, T_{cdo} is the condenser water leaving temperature, T_{cdi} is the condenser water entering temperature, and c_p is the specific heat of water.

With the exception of the refrigerant mass flow rate, which can be measured directly or calculated indirectly using chiller onboard measurements, all parameters on the right side of Equation 4 are known. If $\dot{m}_r$ can be predicted, then $\dot{m}_{cond}$ can be calculated according to Equation 4.

In order to obtain the refrigerant mass flow rate, a predicted model was developed according to the following equations:

$$W_{ac} = aW_{th} + b, \tag{5}$$

$$W_{th} = \dot{m}_{pr} \times (h_{dis} - h_{suc}), \tag{6}$$

where W_{ac} is the actual compressor power input, W_{th} is the theoretical compressor power input, $\dot{m}_{pr}$ is the predicted refrigerant mass flow rate, h_{dis} is the refrigerant enthalpy at the compressor outlet, and h_{suc} is the refrigerant enthalpy at the compressor inlet.

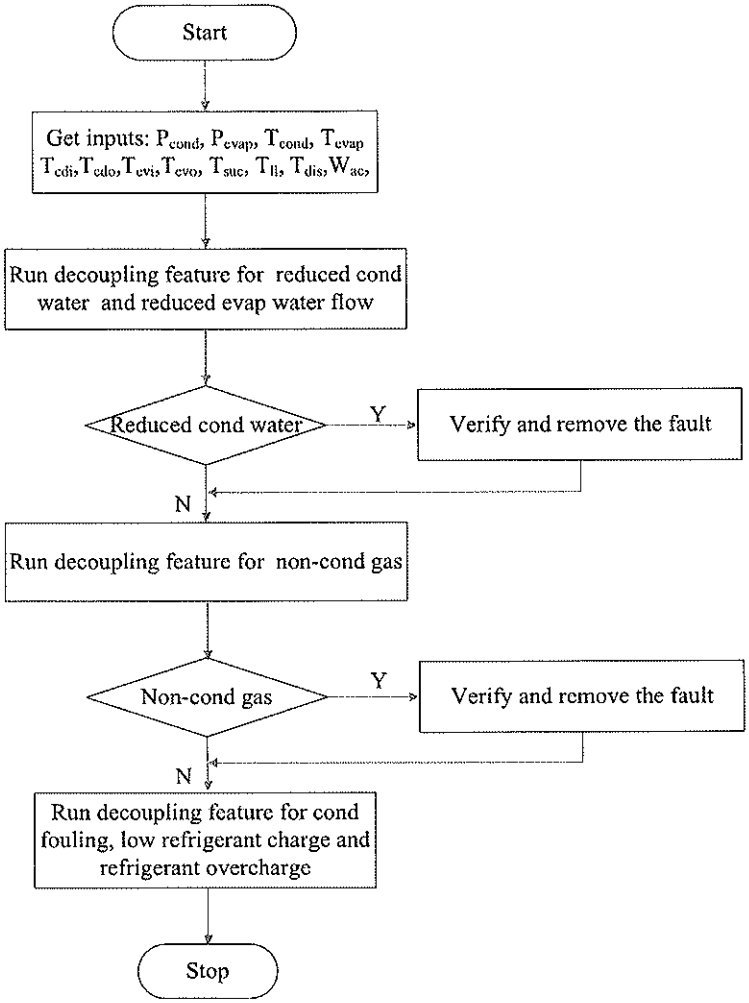

Figure 3. Decoupling-based FDD implementation sequence.

The coefficients used in Equation 5 were obtained from nine operating points of the "Normal 2" benchmark test in the 1043-RP project. Considering the implementation in the field, the structure of nine selected operating conditions is similar to that in chiller manufacturers' rating output table (Table 1). Table 1 lists an example of chiller manufacturer's rating output table. One could get a similar table from the submittals of the chiller or the chiller manufacturer. In the first column of Table 1, the manufacturer lists load conditions from 10% to 100% load. The water temperatures at the condenser inlet, T_{cdi}, and the water temperatures at the evaporator outlet, T_{evo}, are specified conditions. The fourth and fifth columns of the table list the volume flow rates of cooling water through the condenser and chilled water through the evaporator, respectively. W_{ac} is the power input required by the compressor, and P_{cond} and P_{evap} are the refrigerant pressure of the condenser and evaporator, respectively. The final two columns show the condenser subcooling and compressor suction superheat for each of these rating conditions, respectively.

The nine operating points consist of three chiller loads (30%, 60%, and 100%), three water temperature at the condenser inlet (29.4°C [85°F], 23.9°C [75°F], and 18.3°C [65°F]), and a fixed water temperature at the evaporator outlet (7.2°C [45°F]). As shown in Figure 4, the actual compressor power input was plotted against the theoretical

Table 1. Chiller manufacturers' rating output example.

Percent load	T_{cdi} (°C (°F))	T_{evo} (°C (°F))	FWC (L/S (cfm))	FEW (L/S (cfm))	W_{ac} (kW)	P_{cond} (Kpa (psi))	P_{evap} (Kpa (psi))	T_{sc} (°C (°F))	T_{sh} (°C (°F))
100	30.0	7.0	104.3	91.6	311.0	821.0	268.0	4.6	0.6
	(86.0)	(44.6)	(1655.6)	(1454.0)		(119.0)	(38.9)	(8.3)	(1.1)
90	27.7	7.0	104.3	91.6	253.3	748.1	269.0	4.2	0.6
	(81.9)	(44.6)	(1655.6)	(1454.0)		(108.5)	(39.0)	(7.6)	(1.1)
80	25.3	7.0	104.3	91.6	211.9	678.3	269.9	3.8	0.6
	(77.5)	(44.6)	(1655.6)	(1454.0)		(98.4)	(39.1)	(6.8)	(1.1)
70	23.0	7.0	104.3	91.6	181.3	615.4	270.9	3.4	0.6
	(73.4)	(44.6)	(1655.6)	(1454.0)		(89.2)	(39.3)	(6.1)	(1.1)
60	20.7	7.0	104.3	91.6	156.8	556.7	271.8	3.0	0.6
	(69.3)	(44.6)	(1655.6)	(1454.0)		(80.7)	(39.4)	(5.4)	(1.1)
50	18.3	7.0	104.3	91.6	135.8	500.1	272.8	2.6	0.6
	(64.9)	(44.6)	(1655.6)	(1454.0)			(39.6)	(4.7)	(1.1)
40	18.3(64.9)	7.0	104.3	91.6	121.9	489.4	273.8	2.2	0.6
		(44.6)	(1655.6)	(1454.0)		(71.0)	(39.7)	(4.0)	(1.1)
30	18.3	7.0	104.3	91.6	106.2	478.7	274.7	1.7	0.6
	(64.9)	(44.6)	(1655.6)	(1454.0)		(69.4)	(39.8)	(3.1)	(1.1)
20	18.3	7.0	104.3	91.6	86.4	467.9	275.7	1.2	0.6
	(64.9)	(44.6)	(1655.6)	(1454.0)		(67.8)	(40.0)	(2.2)	(1.1)
10	18.3	7.0	104.3	91.6	57.7	456.8	276.7	0.6	0.6
	(64.9)	(44.6)	(1655.6)	(1454)		(66.2)	(40.1)	(1.1)	(1.1)

FWC: Condenser water flow rate; FWE: evaporator water flow rate.

compressor power input, and a fitted curve was developed.

The inputs of the refrigerant mass flow rate predicted model include the actual compressor power input, compressor inlet conditions (refrigerant pressure of the evaporator and refrigerant temperature at compressor inlet), and the compressor outlet conditions (refrigerant pressure of the condenser and refrigerant temperature at compressor outlet). The output is the predicted refrigerant mass flow rate.

Figure 5 shows a plot of the predicted refrigerant mass flow rate against the actual refrigerant mass flow rate. In Figure 5, $\dot{m}_{pr}$ is the predicted refrigerant mass flow rate in kg/s, and $\dot{m}_{actual}$ is the actual refrigerant mass flow rate in kg/s. The data

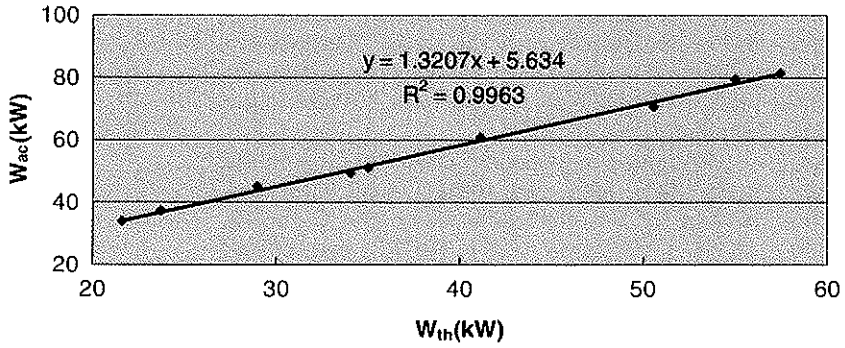

Figure 4. Actual compressor power input vs. theoretical compressor power input (Normal 2 datasets of 1043-RP).

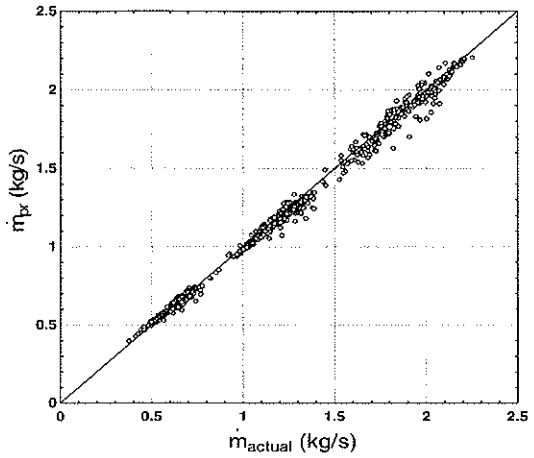

Figure 5. Predicted refrigerant mass flow rate plotted vs. the actual refrigerant mass flow rate.

were obtained from all the fault tests in the 1043-RP project. Except for 5 test data points out of 648, the refrigerant flow rate predicted model estimates are within ±10% of the data. From the predicted results, the refrigerant mass flow rate predicted model could estimate the refrigerant mass flow rate accurately.

According to Equation 4, the condenser water flow rate can be calculated. Therefore, the condenser water flow rate can be predicted by the developed virtual water flow rate meter.

Decoupling feature for reduced evaporator water flow rate fault

Similar to the reduced condenser water flow fault, the evaporator water flow rate could also be predicted by the developed virtual water flow rate meter.

From an energy balance on the evaporator,

$$\dot{m}_{evap} = \frac{\dot{m}_r \times (h_{suc} - h_{ll})}{c_p \times (T_{evi} - T_{evo})}, \qquad (7)$$

where $\dot{m}_r$ is the refrigerant mass flow rate, h_{suc} is the refrigerant enthalpy at compressor inlet, h_{ll} is the saturated liquid enthalpy, $\dot{m}_{evap}$ is the evaporator water flow rate, T_{evi} is the evaporator water entering temperature, and T_{evo} is the evaporator water leaving temperature.

All the parameters other than $\dot{m}_r$ and $\dot{m}_{evap}$ in Equation 7 can be measured directly or calculated indirectly. As described above, $\dot{m}_r$ can be predicted accurately; thus, $\dot{m}_{evap}$ can be calculated according to Equation 7. Therefore, the evaporator water flow rate can also be predicted by the developed virtual water flow rate meter.

As an aid to reader's comprehension, the implementation method of the virtual water flow meter is briefly introduced below.

1. Based on manufacturers' data (Table 1), the condenser heat rejection rate ($Q_{cond} = \dot{m}_{cond} \times c_p \times (T_{cdo} - T_{cdi})$) and the evaporator cooling rate ($Q_{evap} = \dot{m}_{evap} \times c_p \times (T_{evi} - T_{evo})$) can easily be calculated, followed by the theoretical compressor power ($W_{th} = Q_{cond} - Q_{evap}$).
2. Actual compressor power input (W_{ac}) in Table 1 and the theoretical compressor power (W_{th}) are used to obtain the curve fits as in Figure 5.
3. Based on the chiller onboard measurements (refrigerant pressure of the condenser, refrigerant pressure of the evaporator, refrigerant temperature at compressor inlet, refrigerant temperature at compressor inlet, actual compressor power input) and the relationship of theoretical compressor power input and actual compressor power input, the refrigerant mass flow rate can be predicted.
4. Use the refrigerant mass flow rate obtained from Step 4 and the chiller onboard measurements (liquid line temperature; refrigerant pressure of the condenser; refrigerant pressure of the evaporator; refrigerant temperature at compressor inlet; and water temperatures at the condenser inlet, at the condenser outlet, at the evaporator outlet, and at the evaporator outlet) to calculate water flow rate in the condenser loop and evaporator loop.

Decoupling feature for noncondensable gas in system fault

As analyzed above, the noncondensable gas fault is a service fault. This fault is usually introduced into the system during the service period. Therefore, this fault should be diagnosed and fixed during the commissioning period.

When mixed with a two-phase refrigerant, the noncondensable gas exerts a partial pressure that changes the relationship between the refrigerant saturation temperature and total pressure. When noncondensable gas exists in the system, the condensing temperature derived based on the condenser pressure would be higher than the actual condensing temperature. The temperature difference between actual condensing temperature and derived condensing temperature would be a function of pressure

that comes from air in the system. Therefore, the difference between actual condensing temperature and saturation temperature deriving from measured condenser pressure could be used as a decoupling feature for the noncondensable gas fault. A decoupling feature for the noncondensable gas fault was developed to be:

$$\Delta T_{cond} = T_{cond,ms} - T_{cond,cl}, \tag{8}$$

where $T_{cond,ms}$ is actual measured condensing temperature, and $T_{cond,cl}$ is the calculated condensing temperature derived from the condenser pressure with saturation tables. As discussed above, when there is noncondensable gas in the system, the calculated condensing temperature should be higher than the actual measured condensing temperature, so ΔT_{cond} was considered as a decoupling feature to detect and diagnose the noncondensable gas fault in the system.

A natural and straightforward solution for detecting and diagnosing a noncondensable gas fault is to add a temperature sensor inside the condenser shell for comparison with the saturation temperature derived from the condenser pressure measurement. Unfortunately, this measurement is usually not available in centrifugal chillers.

Since there is no refrigerant condensing temperature measurement, a black-box model was developed to describe the relationship between the expected output (condensing temperature) and driving conditions in chiller system. The condensing temperature is assumed to have a function of three driving conditions (condenser heat rejection rate, refrigerant temperature at compressor outlet, and condenser water leaving temperature) that express the operating states of chiller system:

$$\begin{aligned} T_{cond,pr} = {} & a_0 + a_1 Q_{cond} + a_2 Q_{cond}^2 + a_3 T_{dis} \\ & + a_4 T_{dis}^2 + a_5 T_{cdo} + a_6 T_{cdo}^2 \\ & + a_7 T_{cdo} \cdot T_{dis} + a_8 T_{dis} \cdot Q_{cond} \\ & + a_9 T_{cdo} \cdot Q_{cond}, \end{aligned} \tag{9}$$

where $T_{cond,pr}$ is the predicted condensing temperature, Q_{cond} is the condenser heat rejection rate, T_{dis} is the refrigerant temperature at compressor outlet, and T_{cdo} is the condenser water leaving temperature. The coefficients in Equation 9 are determined from the "Normal 2" benchmark test and all fault tests other than the noncondensable gas fault test in the 1043-RP project. As shown in Equation 9, the inputs of the predicted model are condenser heat rejection rate, refrigerant temperature at compressor outlet, and condenser water leaving temperature.

Decoupling feature for condenser fouling fault

Applying heat transfer theory to the condenser,

$$\begin{aligned} Q_{cond} &= \mathrm{UA} \times \frac{\Delta T}{\ln \frac{T_c - T_{cdi}}{T_c - T_{cdo}}} \\ &= \dot{m}_{cond} \times C_p \times \Delta T, \end{aligned} \tag{10}$$

where Q_{cond} is the condenser heat rejection rate, ΔT is the condenser water temperature difference, T_{cdo} is the condenser water leaving temperature, T_{cdi} is the condenser entering temperature, UA is overall heat conductance of heat exchanger, T_c is the refrigerant condensing temperature, c_p is the specific heat of water, and $\dot{m}_{cond}$ is the condenser water flow rate. UA can be expressed as

$$\begin{aligned} \mathrm{UA} &= \dot{m}_{cond} \times C_p \times \ln \frac{T_c - T_{cdi}}{T_c - T_{cdo}} \\ &= \dot{m}_{cond} \times C_p \times \ln \frac{T_c - T_{cdo} + T_{cdo} - T_{cdi}}{T_c - T_{cdo}} \\ &= \dot{m}_{cond} \times C_p \times \ln \left(1 + \frac{\Delta T}{T_c - T_{cdo}} \right). \end{aligned} \tag{11}$$

According to 1275-RP (Reddy 2006), the UA value is an important feature to diagnose the condenser fouling fault. As the severity level of condenser fouling fault increases, the UA value would decrease. So the UA value should be a good indicator for detecting and diagnosing the condenser fouling fault. Unfortunately, the low refrigerant charge fault and the refrigerant overcharge fault also have strong impacts on the UA value. As the severity of the low refrigerant charge fault increases, the UA value increases; as the severity of refrigerant overcharge fault increases, the UA value decreases. So, how to eliminate the impact of refrigerant charge level faults on the UA value is critical to decouple the condenser fouling fault from other faults.

Equation 11 expresses that the UA value is a function of the condenser water temperature difference (ΔT) and the condenser approach temperature (APPR, the difference between the condensing temperature and the leaving water temperature). Table 2 shows the average deviations of ΔT, T_{sc}, and APPR from the normal condition for different faults under four severity levels (1043-RP). As shown in Table 2, when a low refrigerant charge faults, a refrigerant

Table 2. Average deviation of ΔT, T_{sc}, and *APPR* under different faults with four severity levels (SL) in 1043-RP.

Fault	SL1	SL2	SL3	SL4
ΔT				
Reduced condenser water flow	12.4%	26.5%	45.3%	70.2%
Reduced evaporator water flow	1.0%	1.5%	1.6%	1.7%
Low refrigerant charge	–0.4%	–0.6%	–0.1%	–0.1%
Refrigerant overcharge	0.0%	0.7%	4.8%	10.2%
Condenser fouling	0.4%	2.5%	2.8%	6.4%
T_{sc}				
Reduced condenser water flow	10.5%	24.4%	33.9%	61.5%
Reduced evaporator water flow	–0.3%	1.2%	1.5%	2.9%
Low refrigerant charge	0.9%	–4.7%	–35.5%	–66.0%
Refrigerant overcharge	25.7%	32.2%	68.9%	113.1%
Condenser fouling	4.1%	0.1%	4.9%	1.2%
APPR				
Reduced condenser water flow	5.8%	9.1%	7.6%	21.7%
Reduced evaporator water flow	–1.4%	2.8%	2.1%	2.5%
Low refrigerant charge	8.3%	–6.1%	–37.2%	–53.0%
Refrigerant overcharge	39.5%	44.1%	79.0%	129.3%
Condenser fouling	14.8%	14.9%	28.1%	53.8%

Note: SL1 in refers to severity level 1 from 1043-RP.

overcharge fault or condenser fouling fault happens, ΔT varies from –0.6% to 10.2%, while APPR varies from –53.0% to 129.3%. Thus, APPR has a stronger impact on the UA value compared to ΔT. Therefore, the key point to decouple the condenser fouling fault from other faults is to eliminate the influence of the refrigerant charge fault on APPR.

A decoupling feature for the condenser fouling fault was developed as below:

$$UA^* = \dot{m}_{cond} \times C_p \times \ln\left(1 + \frac{\Delta T}{APPR^*}\right). \quad (12)$$

In Equation 12, UA^* is a pseudo condenser overall heat conductance that excludes the influence to which refrigerant charge faults lead. $APPR^*$ is a pseudo condenser approach temperature that eliminates the impact to which refrigerant charge faults result. $APPR^*$ can be calculated as

$$APPR^* = APPR - APPR_{ref}, \quad (13)$$

where $APPR$ is actual approach temperature, and $APPR_{ref}$ is the variation of approach temperature to which refrigerant charge faults lead. $APPR_{ref}$ is identified by following formula:

$$APPR_{ref} = \Delta T_{sc}^* K_{sc,appr}, \quad (14)$$

where ΔT_{sc} denotes the deviation of subcooling from the normal condition. $K_{sc,appr}$ value was determined from the refrigerant charge fault tests datasets in project 1043-RP, which denotes the relationship between subcooling and condenser approach temperature. (Note that the $K_{sc,appr}$ value was obtained from the refrigerant charge fault tests datasets in project 1043-RP, which is not easy to get in the field. The $K_{sc,appr}$ value could be trained to find the relationship between subcooling and condenser approach temperature using manufacturers' data, and the value may be required to tune in field's implementation.) It can be seen from Table 2 that refrigerant charge faults have significant influences on subcooling. Subcooling is a good indicator to flag the refrigerant charge faults and to reflect the severity level of refrigerant charge faults. Thus, $APPR_{ref}$ could indirectly indicate the impact of refrigerant faults on the condenser approach. Once the impact of refrigerant faults on approach temperature is eliminated successfully, the condenser fouling fault could be decoupled from other faults by UA^*.

System-level faults decoupling

The refrigerant charge fault is one of the most problematic issues for HVAC&R systems. Improper charge faults can be introduced during initial

Table 3. Subcooling and superheat of 3-ton R-410A split unit using TXV under different outdoor temperatures (Shen 2006).

	Measurements (°C (°F))					
Outdoor Temperature	28.30 (82.94)	36.05 (96.89)	41.78 (107.20)	47.09 (116.76)	49.96 (121.93)	52.64 (126.75)
T_{sc}	7.79 (14.02)	8.04 (14.47)	7.60 (13.68)	7.82 (14.08)	7.26 (13.07)	7.43 (13.37)
T_{sh}	4.43 (7.97)	4.54 (8.17)	4.19 (7.54)	4.59 (8.26)	4.18 (7.52)	4.43 (7.97)

installation or developed during routine operation. Physically, a low refrigerant charge and refrigerant overcharge fault cannot happen simultaneously; therefore, there is no coupling among these two faults.

Decoupling feature for a low refrigerant charge fault

Li and Braun (2007b) developed a feature for refrigerant charge that is expressed as

$$\Delta T_{sc-sh} = (T_{sc} - T_{sc,rated}) - \frac{K_{sh}}{K_{sc}}(T_{sh} - T_{sh,rated}), \quad (15)$$

where T_{sc} and T_{sh} are liquid line subcooling and suction line superheat. $T_{sc,rated}$ and $T_{sh,rated}$ are the system subcooling and superheat at the rating conditions for the air conditioner. The ratio K_{sh}/K_{sc} is the slope of a straight line plot of $(T_{sc}-T_{sc,rated})$ vs. $(T_{sh}-T_{sh,rated})$. The refrigerant charge feature of Equation 15 is positive for refrigerant overcharge and negative for refrigerant undercharge. The magnitude of the deviation from zero is an indication of the fault severity. For a package unit system with a fixed orifice expansion device, Equation 15 implies that subcooling would increase when superheat increases for a given refrigerant charge. For a package unit system with a thermostatic or electric expansion valve, the superheat is relatively constant, and therefore, Equation 15 denotes that subcooling is almost constant for a given charge. Table 3 is the test data of a 3-ton R-410A split unit using a thermal expansion value (TXV) as an expansion device (Shen 2006). Table 3 shows that superheat is relatively constant for a given charge, and subcooling is also nearly constant under different driving conditions.

Li and Braun (2007b) demonstrated that the refrigerant charge feature has very good performance on package unit system. However, this feature cannot be applied directly to the centrifugal chiller system. For a centrifugal chiller with a TXV device, the suction superheat is relatively constant under different driving conditions because the thermal expansion valve maintains a constant superheat as the load changes. However, the amount of subcooling in the condenser is not constant under different load conditions. It was noted that condenser subcooling has a linear relationship with percent of maximum chiller capacity. Figure 6 shows the subcooling under different chiller load conditions. The data are from the "Normal 2" benchmark test in the 1043-RP

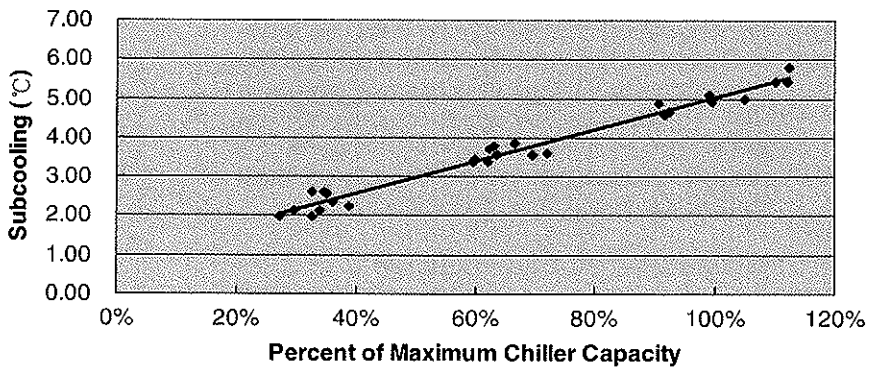

Figure 6. Subcooling vs. percent of maximum chiller capacity (Normal 2 datasets of 1043-RP).

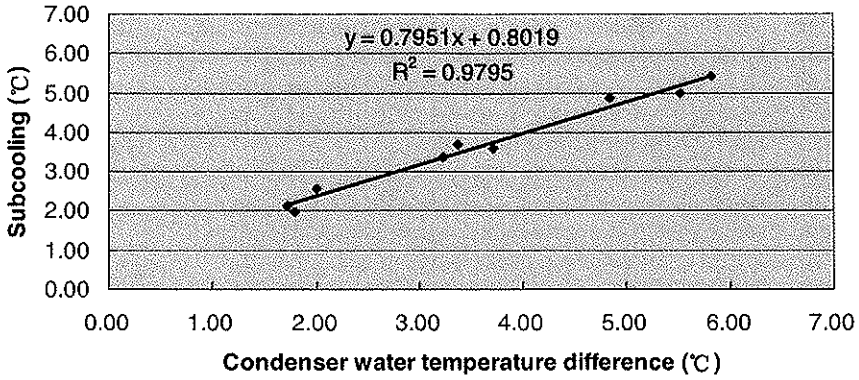

Figure 7. Dependence of T_{sc} on condenser water temperature difference.

project. "Normal 2" is one of the fault-free benchmark tests from 1043-RP. The test was performed at 27 different operation conditions of chiller capacity and operating temperatures, which was identified the best benchmark data among several fault-free datasets by 1275-RP (Reddy 2006). It can be seen in Figure 6 that subcooling increases linearly as the percent of maximum chiller capacity.

In centrifugal chillers, the inlet guide vane is usually used to control the capacity of the compressor. The compressor capacity is modulated by automatic adjustment of prerotation vanes that whirl the refrigerant gas at the impeller eye. With load condition changes, the suction vanes, located just in front of the centrifugal impeller eye, would be in degrees of opening or closure to control the mass flow of refrigerant pumped through the compressor. When they are closed, very likely at lower load point, there would be a small center opening that allows a small amount of refrigerant through the compressor. Meanwhile, the TXV would open widely to ensure the evaporator to be flooded with the majority of the refrigerant, thereby causing less subcooling in the condenser. Therefore, the amount of subcooling in the condenser at rating conditions has strong relationship with refrigerant flow rate in the system. In other words, subcooling is not constant at different rating conditions. Therefore, decoupling features for refrigerant charge level faults in package units cannot be applied directly to centrifugal chiller system. A modified decoupling feature for low refrigerant charge fault in centrifugal chillers is expressed below:

$$\Delta T_{sc-sh}^{-} = (T_{sc} - T_{sc,rated}^{*}) - \frac{K_{sh}}{K_{sc}}(T_{sh} - T_{sh,rated}^{*}), \quad (16)$$

where $T^{*}_{sc,rated}$ and $T^{*}_{sh,rated}$ in Equation 16 are predictions determined from the model, describing how rated subcooling and superheat vary under different driving conditions.

How to identify subcooling and superheat at rating conditions is critical to the modified decoupling feature for refrigerant charge faults in centrifugal chillers. It was noted that the subcooling under rating conditions has a linear relation with the condenser water temperature difference. As shown in Figure 7, subcooling at rating conditions is a strong linear function of condenser water temperature difference. The coefficients in the regression model of Figure 7 are determined from the nine data points of the "Normal 2" benchmark test in the 1043-RP project.

The condenser water temperature difference is considered as the best driving condition for estimating $T^{*}_{sc,rated}$ at normal refrigerant charge level because of the following reasons.

1. As stated above, for a given heat exchanger, subcooling is highly related to refrigerant flow rate in the system. For a centrifugal chiller system, the inlet guide vane is usually used to control the capacity of compressor by modulating the refrigerant mass flow rate through the compressor. The refrigerant mass flow rate increases linearly with increasing load condition. When the condenser water flow rate is constant, the condenser water temperature difference would be a good indicator to reflect the variations of load conditions. Therefore, subcooling is a function of the condenser water temperature difference.
2. For a given heat exchanger, subcooling is also influenced by the condenser water flow rate. At a given load condition, when the condenser

water flow rate reduces, the condenser water temperature difference would increase. A higher condenser water temperature difference tends to cause a higher temperature difference between the water and the condensing refrigerant, which tends to improve the heat transfer effectiveness. Therefore, less area is needed for condensing region, more area can be provided for subcooling. So, at a given load condition, the subcooling also varies linearly with changing of condenser water flow rate.

3. From the implementation cost point of view, the condenser temperature difference is readily obtained from the on-board measurements of centrifugal chillers. Thus, the condenser temperature difference is a good regressor for predicting the amount of subcooling at normal refrigerant charge level.

Based on the above analysis, $T^*_{sc,rated}$ is associated with variations of the refrigerant flow rate and the condenser water flow rate. The condenser water temperature difference has a strong relationship with the refrigerant flow rate and the condenser water flow rate. Therefore, it was selected as a good regressor to estimate subcooling at normal refrigerant charge under different driving conditions.

For a centrifugal chiller with a TXV, the suction superheat is nearly constant. Therefore, $T^*_{sh,rated}$ can be obtained easily from the manufacturers' rating data sheets. In this study, a mean suction superheat is determined from the datasets of the "Normal 2" benchmark test in the 1043-RP project.

For a system using a TXV as the expansion device, the suction superheat only fluctuates around the rating value over a relatively small range. In this case, it is not possible to estimate the ratio of $-K_{sh}/K_{sc}$, since (K_{sh}/K_{sc}) * $(T_{sh}-T_{sh,rated}) \approx (T_{sh}-T_{sh,rated}) \approx 0$. Li and Braun (2009b) employed an empirical value of K_{sh}/K_{sc} equal to 1/2.5. In order to evaluate this ratio, the feature of $\Delta T_{sc\text{-}sh}$ was tested using fault-free data and faulty data under four severity levels (specifically, Normal 2, reduced evaporator water flow, reduced condenser water flow, and condenser fouling) containing 361 observations. The ration of K_{sh}/K_{sc} was set as 1/2.5. The results show that the average of 361 data points is 0.02; the standard deviation is about 0.3. For a system with a normal charge, $\Delta T_{sc\text{-}sh}$ should be constant at about zero. The tolerance limits of 361 measurements were also calculated, and the results shows that the upper tolerance limit is 1.02°C (1.84°F) and the lower tolerance limit is −0.98°C (−1.76°F), which means 99% of the measurements fall in the range from −0.98°C (−1.76°F) to1.02°C (1.84°F) with a 95% confidence level. From the test results, it is reasonable to set the ratio of K_{sh}/K_{sc} as 1/2.5 for implementing the feature.

The low refrigerant charge feature shown in Equation 16 is relatively dependent on the refrigerant charge; it is negative for low refrigerant charge. The magnitude of the deviation from zero is an indication of the severity level of the low refrigerant charge fault.

Decoupling feature for refrigerant overcharge level fault

A modified decoupling feature for refrigerant overcharge fault is expressed below:

$$\Delta T^{+}_{sc-sh} = (T_{sc} - T^*_{sc,rated}) - \frac{K_{sh}}{K_{sc}}(T_{sh} - T^*_{sh,rated}). \quad (17)$$

The refrigerant overcharge feature of Equation 17 is positive for refrigerant overcharge. The magnitude of the deviation from zero is an indication of the severity level of the refrigerant overcharge fault.

Validation of decoupling features for centrifugal chiller

The datasets from ASHRAE 1043-RP (Comstock and Braun 1999) were used to evaluate the performance of proposed decoupling features for common faults that happened on centrifugal chillers. The scope of this study was limited to six common faults: reduced condenser water flow fault, reduced evaporator water flow fault, low refrigerant charge fault, refrigerant overcharge fault, condenser fouling fault, and noncondensable gas fault. In the real world, there may be other faults that could impact the proposed decoupling features; this issue is not considered in this work. In 1043-RP, six common individual faults were artificially introduced at different fault severity levels (see Table 4), and the unit was tested at 27 different operating conditions of chiller load (low load, 30%; medium load, 50%–60%; high load, 100%), evaporator water leaving temperature, and condenser water entering temperature. Although fault tests in 1043-RP are individual fault tests instead of multiple simultaneous faults test, they could also be used to test whether the proposed decoupling features for each fault are independent of driving conditions and all other chiller faults.

Table 4. Fault levels introduced to six chiller faults

Fault level	Reduced condenser water	Reduced evaporator water	Low refrigerant charge	Refrigerant overcharge	Condenser fouling	Noncondensable gas
0	0	0	0	0	0	0
1	10%	10%	10%	10%	12%	1%
2	20%	20%	20%	20%	20%	1.7%
3	30%	30%	30%	30%	30%	2.4%
4	40%	40%	40%	40%	45%	5.7%

Validation of decoupling features for reduced condenser water flow rate fault

In order to quantify the severity of condenser water flow rate fault, the normalized condenser water flow rate was chosen as a feature for decoupling the reduced condenser water flow rate fault. The normalized condenser water flow rate is defined as

$$\text{Normalized condenser water flow rate} = \frac{\text{Predicted condenser water flow rate}}{\text{Designed condenser water flow rate}}.$$

Figure 8 shows the normalized condenser water flow rate, which is estimated using the developed virtual water flow meter under different fault types and load levels. It can be seen from Figure 8 that the feature is only influenced by the reduced condenser water flow rate fault. The reduction of condenser water flow rate is proportional to the fault level and independent of other faults. Thus, decoupling between the reduced condenser water flow rate fault and other faults was achieved.

Figure 9 shows filtered results for the normalization of the estimated condenser water flow rate for different faults and load levels. The average of nine steady-state data points for each load condition (low, medium, and high) were plotted to show the performance of decoupling feature. The same method was also used in evaluating other decoupling features. Each validation of other decoupling features in this article contains a figure similar to Figure 9.

It shows more clearly in Figure 9 that decoupling for the reduced condenser water flow rate fault is achieved successfully. The feature is sensitive to the reduced condenser water flow fault; 15%–20% water flow reduction can be detected by this feature. All the faults other than the reduced condenser water flow rate fault have little impact on the feature.

Validation of decoupling features for reduced evaporator water flow rate fault

Like the reduced condenser water flow rate, the normalized evaporator water flow rate was chosen as a decoupling feature for the reduced evaporator

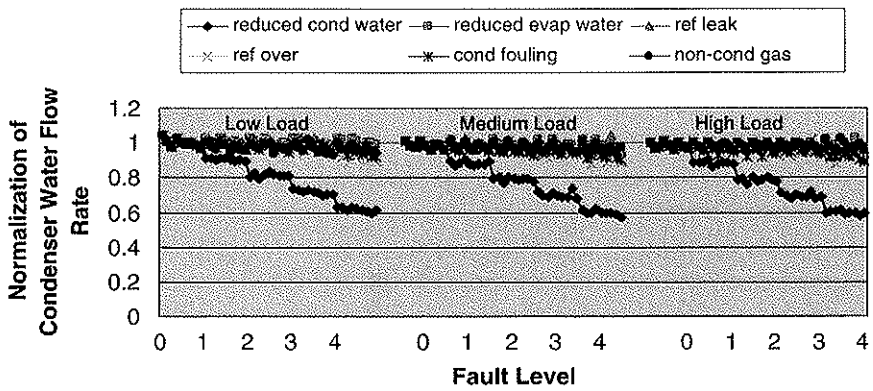

Figure 8. Decoupling reduced condenser water flow rate fault using normalized predicted condenser water flow rate.

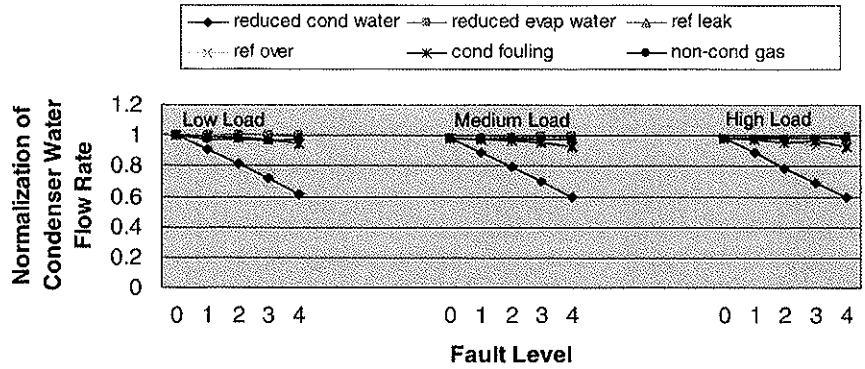

Figure 9. Filtered results for reduced condenser water flow rate fault decoupling.

water flow rate fault. The normalized evaporator water flow rate is defined as

$$\text{Normalized evaporator water flow rate} = \frac{\text{Predicted evaporator water flow rate}}{\text{Designed evaporator water flow rate}}.$$

Figure 10 shows the normalization of the estimated evaporator water flow rate, which is calculated using the developed virtual flow meter under different fault types and load levels. It can be seen from Figure 10 that the feature is only influenced by the reduced evaporator water flow rate fault. The reduction of the evaporator water flow rate is proportional to the fault level and independent of other faults. Therefore, the decoupling between the reduced evaporator water flow rate fault and other faults is fully achieved.

Figure 11 shows the filtered results of the normalization of the estimated evaporator water flow rate for different faults and load levels. It can be seen clearly that coupling between the reduced evaporator water flow rate fault and other faults is achieved. The filtered results show that the developed virtual water flow meter has good and robust performance in monitoring the water flow rate in the water loop of the chiller system.

Validation of decoupling features for noncondensable gas fault

Figure 12 illustrates the performance of ΔT_{cond} for different fault types with different fault levels and load conditions. It can be seen from Figure 12 that the noncondensable gas fault has a significant influence on the feature ΔT_{cond}, while other faults have small impacts on it. It can be seen that, in addition to several data points, the ΔT_{cond} value of all the faults other than the noncondensable gas fault is basically within $\pm 1°C$ (1.8°F). The exceptional data points may be caused by measurements noise

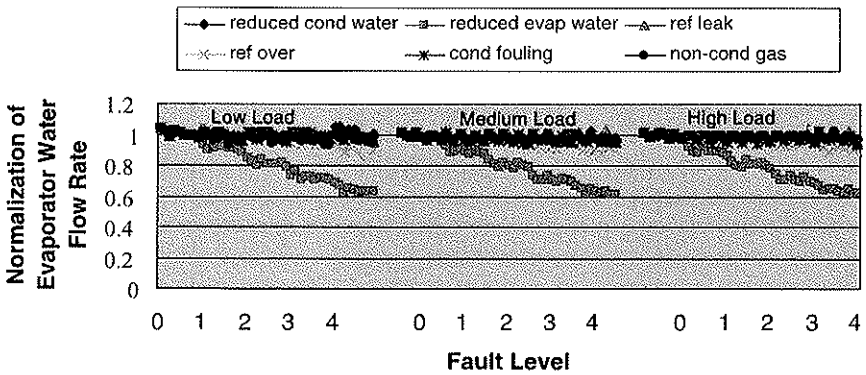

Figure 10. Decoupling reduced evaporator water flow rate fault using normalized predicted evaporator water flow rate.

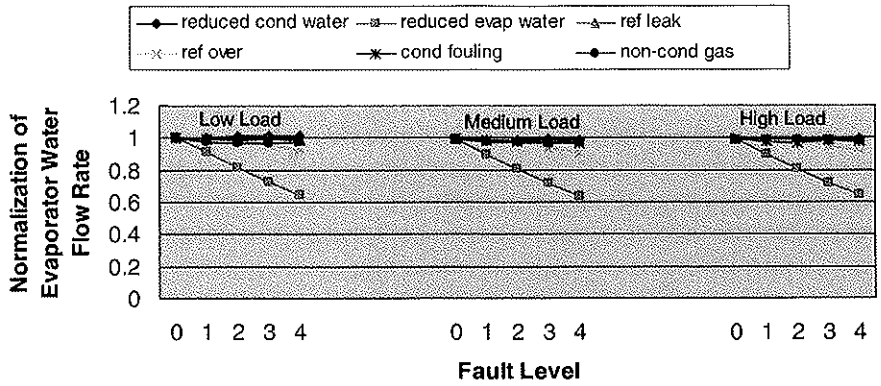

Figure 11. Filtered results for reduced evaporator water flow rate fault decoupling.

or modeling error. This issue can be eliminated or relieved by using the mean theorem.

Figure 13 shows filtered results for noncondensable gas fault decoupling. From Figure 13, it can be seen that after the filtering process, the exception data points disappear, and the ΔT_{cond} value of all the faults other than noncondensable gas fault is within ±1°C (1.8°F). The feature of ΔT_{cond} was evaluated using normal test data and faulty data under four severity levels (specifically, Normal 2, reduced evaporator water flow, reduced condenser water flow, low refrigerant charge, and refrigerant overcharge condenser fouling) containing 567 observations. The results show that the average of 567 data points is –0.03°C (–0.05°F); the standard deviation is about 0.39°C (0.7°F); the upper tolerance limit is 0.98°C (1.76°F); and the lower tolerance limit is –1.04°C (–1.87°F), which means 99% of the measurements fall in the range from –1.04°C (–1.87°F) to 0.98°C (1.76°F) with a 95% confidence level. It can be seen from Figure 9 that the ΔT_{cond} value is influenced primarily by the noncondensable gas fault. With the severity level of the noncondensable fault aggravates, the magnitude of the deviation from zero increases. The ΔT_{cond} value for the noncondensable gas fault with different faults and load levels is basically less than –1.5°C (–2.7°F). Only at high load conditions of the noncondensable gas fault under a lower fault level (fault level 2) was the ΔT_{cond} value larger than –1°C (–1.8°F). This small fluctuation may be caused by system disturbances or modeling error. Such small fluctuations would not change the performance of the decoupling feature. Therefore, decoupling between noncondensable gas fault and other faults is basically achieved.

Validation of decoupling features for condenser fouling fault

Similar to the analysis in the validation of ΔT_{cond}, the normalized feature value of UA^* (UA^* is divided by normal the UA value, which is a mean value from

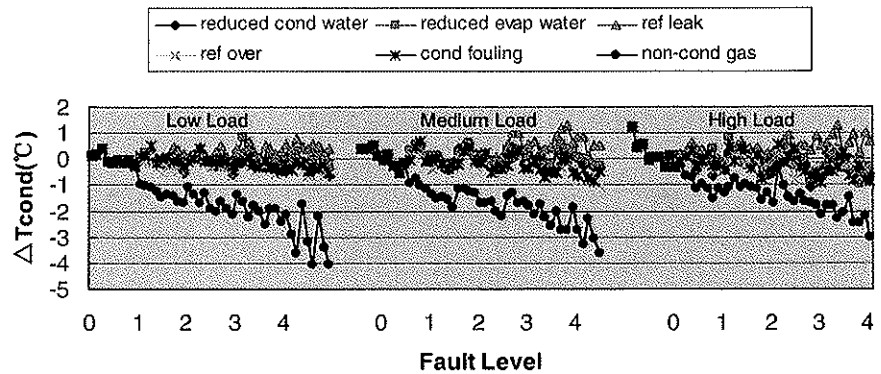

Figure 12. Decoupling noncondensable gas in refrigerant fault using ΔT_{cond}.

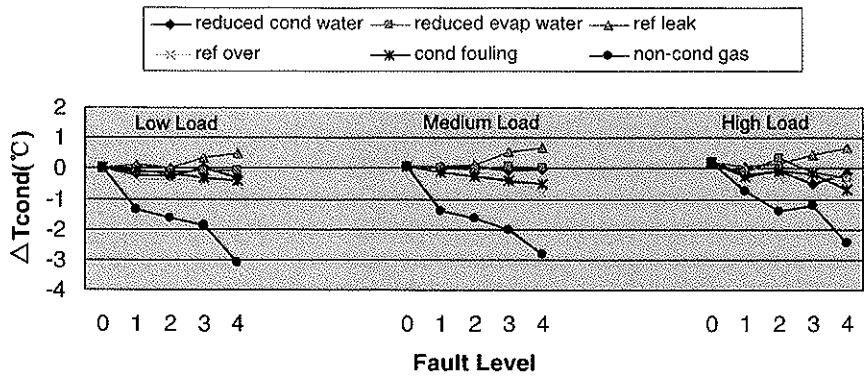

Figure 13. Filtered results for noncondensable gas fault decoupling.

"Normal 2" of 1043-RP) was also evaluated using normal test data and faulty data under four severity levels (specifically, Normal 2, reduced evaporator water flow, low refrigerant charge, and refrigerant overcharge) containing 361 observations. The results show that the average of 361 data points is 0.96; the standard deviation is about 0.08; the upper tolerance limit is 1.18, and the lower tolerance limit is 0.74, which means 99% of the measurements fall in the range (0.74, 1.18) with a 95% confidence level.

Figure 14 shows the performance of the decoupling feature for the condenser fouling fault. Since subcooling would be overstated when there is noncondensable gas in the system, an assumption was made that there is no noncondensable gas in the system. The assumption is reasonable because the noncondensable gas fault can be flagged and removed during the commissioning period. The same assumption was also made when the decoupling feature of ΔT^{-}_{sc-sh} and ΔT^{+}_{sc-sh} were evaluated.

From Figure 14, the decline trend of the *UA** value is expected for the condenser fouling fault. When the severity level of the condenser fouling fault increases, the *UA** value decreases. In terms of FDD sensitivity, the feature shows poor performance in detecting the condenser fouling fault. At lower fault levels, the condenser fouling fault can barely be detected by the feature. Only at fault level 4 does the feature work (about 25% reduction compared with fault-free condition). According to 1275-RP (Reddy 2006), fault level 4 of the condenser fouling fault would cause a 1.8% energy penalty. Therefore, in the sense of practical use, the low FDD sensitivity of the feature would not affect the FDD implementation.

Figure 14 also reveals that the reduced condenser water flow rate fault and the low refrigerant charge fault have some impacts on this feature. The impact from the reduced condenser water flow rate fault was expected, since the condenser water flow rate does have a strong influence on this feature. However,

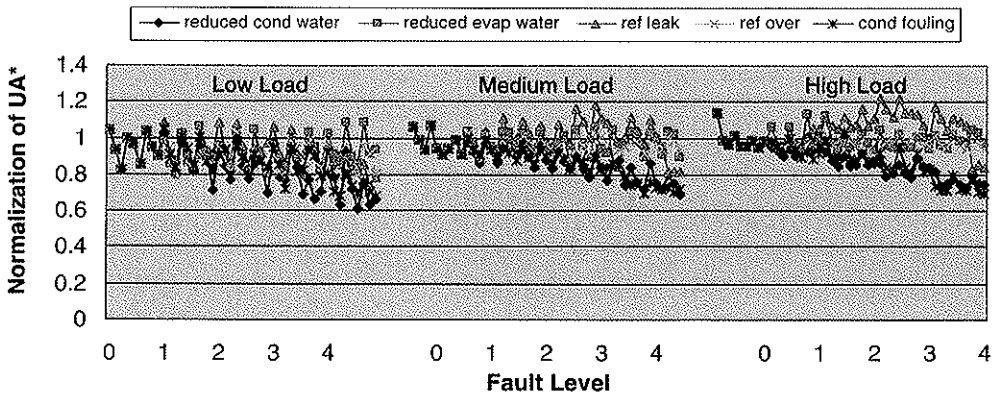

Figure 14. Decoupling condenser fouling fault using *UA**.

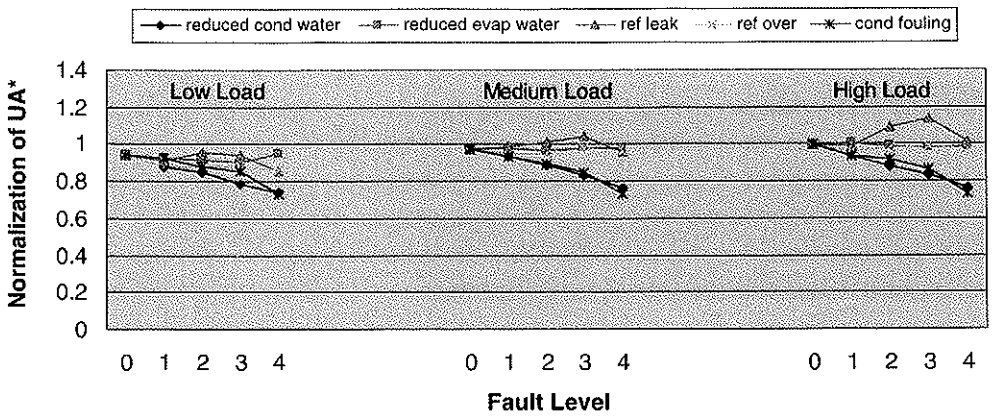

Figure 15. Filtered results for condenser fouling fault decoupling.

this would not affect the FDD application, because it was demonstrated that the decoupling feature for the reduced condenser water flow rate is not affected by the condenser fouling fault, so partial decoupling could relieve or solve this problem. For the impact from the low refrigerant charge fault, the fluctuation of the UA^* value may be caused by the measurement noise or modeling error.

Figure 15 shows the filtered results of UA^* for different fault types, fault severity levels, and load conditions. In the filtered results, it can be seen that the impact from the low refrigerant charge fault greatly decreases. At fault level 4, the UA^* value is primarily influenced by the condenser fouling fault and the reduced condenser water flow rate fault. The condenser fouling fault could be detected successfully by the feature. Therefore, a partial decoupling for the condenser fouling fault can be achieved in terms of FDD application.

Validation of decoupling features for low refrigerant charge fault

Figure 16 shows the performance of the decoupling feature (ΔT_{sc-sh}^{-}) for the different faults and load levels. It can be seen from Figure 16 that ΔT_{sc-sh}^{-} is primarily influenced by the low refrigerant charge fault. With the severity level of low refrigerant charge fault aggravates, the magnitude of the deviation from zero increases. In Figure 16, it can also be seen that ΔT_{sc-sh}^{-} shows better performance when the chiller runs at medium and high load conditions. As analyzed above, subcooling has a strong relationship with load conditions. With load conditions decreases, subcooling would drop accordingly. At the low load condition (30% load), subcooling at rating condition is only about 2°C. Such low subcooling would affect the performance of ΔT_{sc-sh}^{-}, since centrifugal chillers also spend some of the time

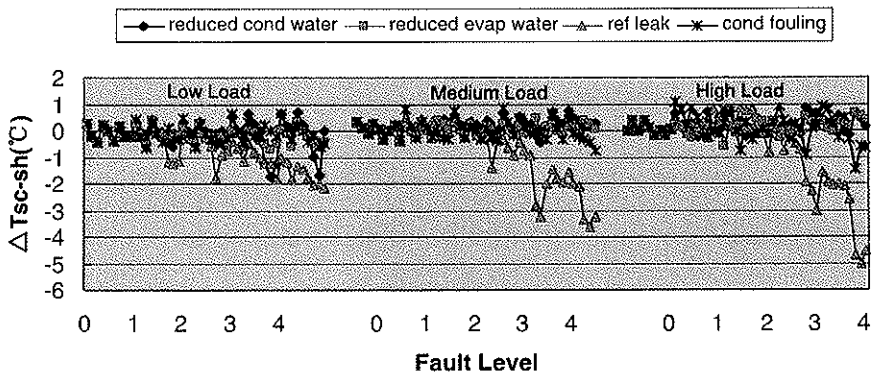

Figure 16. Decoupling low refrigerant charge fault using ΔT_{sc-sh}^{-}.

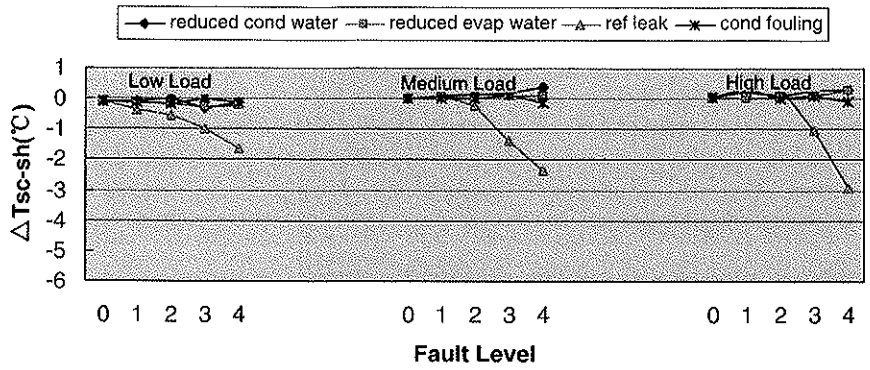

Figure 17. Filtered results for low refrigerant charge fault decoupling.

running at medium condition and high load conditions. Therefore, this is not a problem in terms of FDD application. The low refrigerant charge fault can still be detected and diagnosed by the developed feature when chillers run at medium load condition and high load condition.

From the FDD sensitivity point of view, it can be seen from Figure 16 that the refrigerant charge is undercharged by 20%, which could hardly be detected and diagnosed. Grace et al. (2005) conducted an experimental investigation on the effect of refrigerant charge level on the performance of a chiller system and indicated that a large chiller could work over a wide range of charge levels, 25% below and 25% above the design charge level, without significant impact on its performance. Fortunately, the proposed decoupling feature for the refrigerant charge fault could provide steady and accurate FDD results when the charge level deviates from normal charge by –30% (fault level 3).

Figure 16 also shows that ΔT_{sc-sh}^{-} is slightly impacted by reduced condenser water fault and condenser fouling fault at higher fault levels. These small impacts may be caused by modeling error or measurement noise. Figure 17 shows the filtered results of ΔT_{sc-sh}^{-} for the different faults and load levels. In the filtered results, it can clearly be seen that the coupling from low refrigerant charge fault to other faults is broken. All faults other than refrigerant charge faults have small impacts on this feature.

Validation of decoupling features for refrigerant overcharge fault

Figure 18 shows the performance of the decoupling feature (ΔT_{sc-sh}^{+}) for different fault types, fault levels, and load conditions. It can be seen from Figure 18 that the refrigerant overcharge fault has a considerable influence on the refrigerant overcharge feature. When refrigerant overcharge fault occurs, the value of ΔT_{sc-sh}^{+} is positive. With severity level of refrigerant overcharge aggravates, the magnitude of the deviation from zero increases. All the other

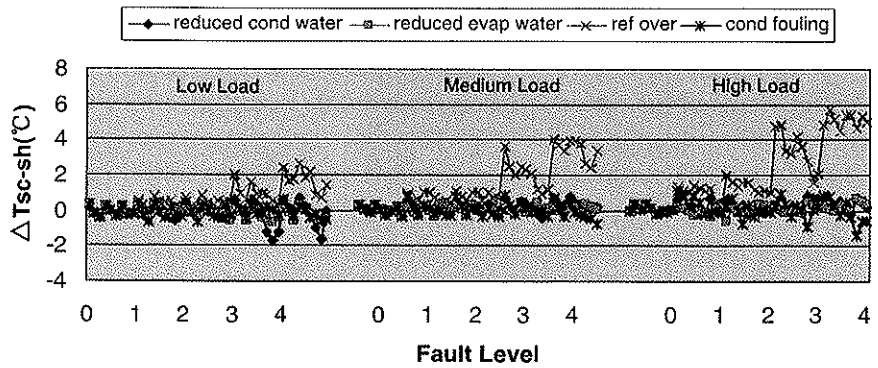

Figure 18. Decoupling refrigerant overcharge fault using ΔT_{sc-sh}^{+}.

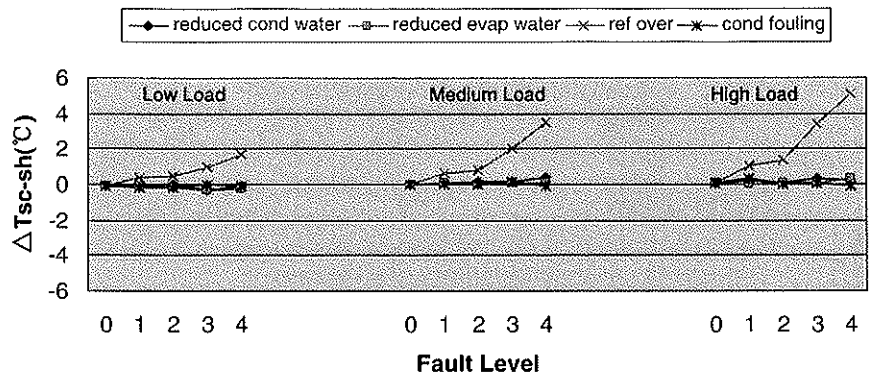

Figure 19. Filtered results for refrigerant overcharge fault decoupling.

faults have little impact on the feature. For the same reason as low refrigerant charge fault, the decoupling feature for refrigerant overcharge fault shows poor performance when the chiller runs at low load condition. Fortunately, this feature works at medium and high load conditions.

Figure 19 also illustrates the filtered results of ΔT^{+}_{sc-sh} for different faults, fault levels, and load levels. It can be seen from Figure 19 that the coupling from the refrigerant overcharge fault to other faults is broken. All the other faults have little impact on this feature. The value of ΔT^{+}_{sc-sh} is proportional to refrigerant overcharge fault level. Similar to the results of the low refrigerant charge fault test, the developed decoupling feature is sensitive for refrigerant overcharge fault when the system is overcharged by above 30% (fault level 3).

Conclusions and discussions

Based on the decoupling methodology proposed by Li and Braun (2007a), several decoupling features for centrifugal chillers were developed in this study. The decoupling features for different chiller faults were developed based on a comprehensive understanding of chiller system, faults cause, faults impact, and cost consideration. The rich onboard measurements of the chiller system were exploited to develop the decoupling features for different chiller faults. The performance of the decoupling features was tested and validated with the laboratory data from a 90-ton centrifugal chiller tested in a laboratory environment. The validation results show that the couplings among different centrifugal chiller faults can be broken fully or partially by the developed decoupling features.

In terms of application, the proposed decoupling features lay a strong basis for detecting and diagnosing multiple simultaneous faults occurring on centrifugal chillers. These decoupling features could be combined together as a chiller FDD tool to be integrated into the controllers in chillers to monitor and diagnose faults. Each of developed decoupling features could also be implemented as an individual virtual sensor to automatically monitor some important parameters of chiller system. For example, the developed virtual water flow meter in this study shows good performance in indicating the water flow rate in the water loop of chiller system. Therefore, it could replace the actual water flow sensor on chillers so as to reduce the expensive initial cost and maintenance cost.

The scope of this research has been limited to the chiller type in 1043-RP. The developed decoupling features may be required to adjust and tune to adapt to different chiller type, design, and controls.

Nomenclature

$APPR$	= condenser approach temperature
$APPR^{*}$	= pseudo condenser approach temperature that excludes the impact of refrigerant charge faults
$APPR_{ref}$	= variation of approach temperature to which refrigerant charge faults lead
c_p	= specific heat of water at constant pressure
h_{dis}	= refrigerant enthalpy at compressor outlet
h_{ll}	= condenser outlet enthalpy
h_{suc}	= refrigerant enthalpy at compressor inlet
K_{sc}	= slope of refrigerant charge vs. liquid line subcooling

$K_{sc,appr}$ = average ratio of subcooling vs. condenser approach
K_{sh} = the slope of refrigerant charge vs. suction line superheat
$\dot{m}_{cond}$ = condenser water flow rate
$\dot{m}_{evap}$ = evaporator water flow rate
$\dot{m}_r$ = refrigerant mass flow rate
$\dot{m}_{pr}$ = predicted refrigerant mass flow rate
P_{cond} = refrigerant pressure of the condenser
P_{evap} = refrigerant pressure of the evaporator
Q_{cond} = condenser heat rejection rate
Q_{evap} = evaporator cooling rate
T_{cdi} = water temperature at the condenser inlet
T_{cdo} = water temperature at the condenser outlet
$T_{cond,cl}$ = calculated condensing temperature that derived from condenser pressure with saturation tables
$T_{cond,ms}$ = actual measured condensing temperature
$T_{cond,pr}$ = predicted condensing temperature
T_{dis} = refrigerant temperature at compressor outlet
T_{evi} = water temperature at the evaporator inlet
T_{evo} = water temperature at the evaporator outlet
T_{ll} = liquid line temperature
T_{sc} = liquid line subcooling
$T_{sc,rated}$ = liquid line subcooling at rating condition
$T^*_{sc,rated}$ = model predictions that describe how rated subcooling vary under different driving conditions
T_{sh} = suction line superheat
$T_{sh,rated}$ = suction line superheat at rating condition
$T^*_{sh,rated}$ = model predictions that describe how rated superheat vary under different driving conditions
T_{suc} = refrigerant temperature at compressor inlet
UA = overall heat conductance of heat exchanger
UA^* = pseudo condenser overall heat conductance that excludes the influence of refrigerant charge faults
W_{ac} = actual compressor power input
W_{th} = theoretical compressor power input
ΔT = condenser water temperature difference
ΔT_{cond} = decoupling feature for noncondensable gas
ΔT_{sc} = deviation of subcooling from normal condition
$\Delta T^-_{sc\text{-}sh}$ = decoupling feature for low refrigerant charge fault
$\Delta T^+_{sc\text{-}sh}$ = decoupling feature for refrigerant overcharge

References

Comstock, M.C., and J.E. Braun. 1999. Development of analysis tools for the evaluation of fault detection and diagnostics in chillers. ASHRAE Research Project 1043–RP; also, Ray W. Herrick Laboratories. Purdue University. HL 99–20: Report #4036–3, December.

DOE. 2009. *Buildings Energy Data Book.* Washington, DC: U.S. Department of Energy.

Grace, I.N., D. Datta, and S.A. Tassou. 2005. Sensitivity of refrigerant system performance to charge levels and parameters for on-line leak detection. *Applied Thermal Engineering* 25(5):557–66.

Jia, Y., and T.A. Reddy. 2003. Characteristic physical parameter approach to modeling chillers suitable for fault detection, diagnosis and evaluation. *ASME Journal of Solar Energy Engineering* 125:258–65.

Li, H., and J.E. Braun. 2007a. A methodology for diagnosing multiple-simultaneous faults in vapor compression air conditioners. *HVAC&R Research* 13(2):369–95.

Li, H., and J.E. Braun. 2007b. Decoupling features and virtual sensors for diagnosis of faults in vapor compression air conditioners. *International Journal of Refrigeration* 30(3):546–64.

Li, H., and J.E. Braun. 2009a. Decoupling features for diagnosis of reversing and check valve faults in heat pumps. *International Journal of Refrigeration* 32(2):316–26.

Li, H., and J.E. Braun. 2009b. Development, evaluation, and demonstration of a virtual refrigerant charge sensor. *HVAC&R Research* 15(1):117–36.

Li, H., and J.E. Braun. 2009c. Virtual refrigerant pressure sensors for use in monitoring and fault diagnosis of vapor-compression equipment. *HVAC&R Research* 15(3):597–616.

Reddy, T.A. 2006. Evaluation and assessment of fault detection and diagnostic methods for centrifugal chillers—Phase II. Final project report of ASHRAE Research Project RP-1275, June, Atlanta, GA.

Reddy, T.A. 2007a. Application of a generic methodology to assess four different chiller FDD methods (RP-1275). *HVAC&R Research* 13(5):711–29.

Reddy, T.A. 2007b. Development and evaluation of a simple model-based automated fault detection and diagnosis (FDD) method suitable for process faults of large chillers. *ASHRAE Transactions* 113(2):27–39.

Shen, B. 2006. Improvement and validation of unitary air conditioner and heat pump simulation models at off-design conditions. Ph.D. thesis, Herrick Laboratories, Purdue University.

Wang, S.W., and J.T. Cui. 2006. A robust fault detection and diagnosis strategy for centrifugal chillers. *HVAC&R Research* 12(3):407–28.